EFFECT OF UNMIXING-BASED HYPERSPECTRAL SUPER-RESOLUTION ON TARGET DETECTION

Naoto Yokoya and Akira Iwasaki

Department of Advanced Interdisciplinary Studies, The University of Tokyo, Japan

ABSTRACT

We present an airborne experiment on unmixing-based hyperspectral super-resolution using RGB imagery to examine the restoration of pure spectra comparing with ground-measured spectra and demonstrate its impact on target detection. An extended version of *coupled nonnegative matrix factorization* (CNMF) is used for hyperspectral super-resolution to deal with a challenging problem setting. Our experiment showed that the extended CNMF can restore pure spectra, which contribute to accurate target detection.

Index Terms— Hyperspectral super-resolution, data fusion, unmixing, coupled nonnegative matrix factorization (CNMF)

1. INTRODUCTION

Hyperspectral (HS) imagers generally have a larger ground sampling distance (GSD) than multispectral (MS) imagers owing to a trade-off of sensor design between spatial and spectral resolutions and the signal-to-noise ratio. HS and MS data fusion enables super-resolution of HS data [1, 2, 3]. A Bayesian approach was first proposed for HS super-resolution using MS data [1, 2]. Unmixing-based HS and MS data fusion can enhance the spatial resolution of HS data with little spectral distortion [3]. An unmixing-based HS and MS data fusion method, named *coupled nonnegative matrix factorization* (CNMF), was proposed for remote sensing [3]. CNMF is composed of alternating unmixing for two images using nonnegative matrix factorization (NMF) [4].

HS and MS data can be represented in matrix form as $\mathbf{X} \in \mathbb{R}^{L_h \times P_h}$ and $\mathbf{Y} \in \mathbb{R}^{L_m \times P_m}$, respectively. L_h and L_m denote the numbers of spectral bands, and P_h and P_m denote the numbers of pixels. The high-spatial-resolution HS data to be estimated is denoted as $\mathbf{Z} \in \mathbb{R}^{L_h \times P_m}$. The spectrum at each pixel $\mathbf{z} \in \mathbb{R}^{L_h \times 1}$ is assumed to be a linear combination of several endmember spectra. Therefore, $\mathbf{Z}$ is formulated as

$$\mathbf{Z} = \mathbf{EA} + \mathbf{N}, \qquad (1)$$

where $\mathbf{E} \in \mathbb{R}^{L_h \times M}$ is the endmember matrix and M being the number of endmembers. $\mathbf{A} \in \mathbb{R}^{M \times P_m}$ is the abundance matrix and $\mathbf{N} \in \mathbb{R}^{L_h \times P_m}$ is the residual. Unmixing-based HS and MS data fusion yields estimates of $\mathbf{E}$ and $\mathbf{A}$ from observable $\mathbf{X}$ and $\mathbf{Y}$ to reconstruct $\mathbf{Z}$. The low-spatial-resolution HS data and MS data are modeled as

$$\mathbf{X} = \mathbf{ZS}, \quad \mathbf{Y} = \mathbf{RZ}. \qquad (2)$$

Here, $\mathbf{S} \in \mathbb{R}^{P_m \times P_h}$ is the spatial response transform matrix and $\mathbf{R} \in \mathbb{R}^{L_m \times L_h}$ is the spectral response transform matrix, which are defined as relative sensor characteristics in the spatial and spectral domains, respectively. By substituting (1) into (2) and (3), $\mathbf{X}$ and $\mathbf{Y}$ can be approximated as two LSMMs:

$$\mathbf{X} \approx \mathbf{E}(\mathbf{AS}), \quad \mathbf{Y} \approx (\mathbf{RE})\mathbf{A}. \qquad (3)$$

$\mathbf{E}$ and $\mathbf{A}$ can be obtained by alternating unmixing of $\mathbf{X}$ and $\mathbf{Y}$ under the constraints of the relative sensor characteristics ($\mathbf{R}$ and $\mathbf{S}$). Here, we define $\mathbf{A}_h = \mathbf{AS}$ and $\mathbf{E}_m = \mathbf{RE}$ as degraded versions of $\mathbf{A}$ and $\mathbf{E}$, respectively. Spatial and spectral consistency, which is expressed as $\mathbf{RX} = \mathbf{YS}$ from (2) and (3), is important in practical use.

HS and MS data fusion algorithms in remote sensing have mainly been evaluated using synthetic datasets or real datasets taken from different platforms [5]. In this work, we present an airborne experiment on unmixing-based hyperspectral super-resolution to examine the restoration of pure spectra using ground measurements and show its impact on target detection. An extended CNMF is introduced to deal with a challenging problem setting: only three channels for MS data and a 10-fold GSD difference.

2. MATERIALS AND METHODS

2.1. Image Acquisition and Preprocessing

Airborne observation was conducted using HS and RGB cameras mounted on a small aircraft. The HS camera is a HyperSpec-VNIR-C (Headwall Photonics Inc.), which captures 128 bands in the 390–1040 nm spectral range by push-broom imaging. The 400–800 nm spectral region was used because the remaining wavelength ranges have low accuracy of reflectance conversion. The RGB camera is an EOS 5D Mark II (Canon Inc.). The altitude was approximately 1000 m and the GSDs of the HS and RGB images are 2.5 and
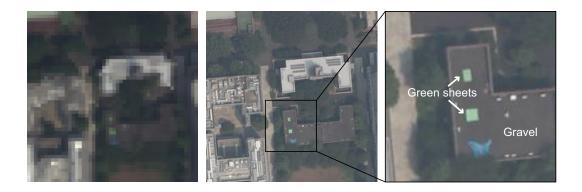
Fig. 1. Color images of study area obtained by (left) HS and (right) RGB cameras.

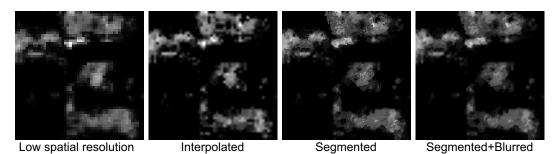| Low spatial resolution | Interpolated | Segmented | Segmented+Blurred |

Fig. 2. Improved initialization of high-spatial-resolution abundance map.

0.25 m, respectively, after geometric projection. The dataset was acquired over the University of Tokyo campus and the neighboring urban area. Fig. 1 shows color images of part of the study area obtained using HS and RGB cameras. We set two green plastic sheets as targets to be detected on a roof of the building where is covered by gravel.
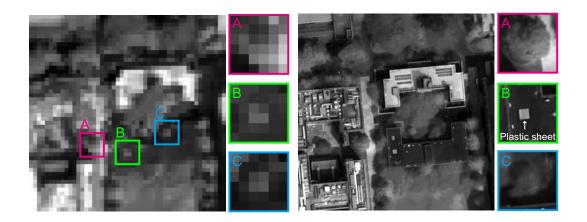
To ensure spatial and spectral consistency between HS and RGB images, the preprocessing is important: (i) *Smile* and *keystone* are modified using an image-matching technique [6]. (ii) Geometric projection is applied to two datasets and the HS image is registered to the RGB image to mitigate geometric errors caused by the difference in scanning type, i.e., line and area scanning. The relative spatial response function ($\mathbf{S}$) can be approximated by a Gaussian filter. (iii) The HS image is converted to a reflectance image using ground-measured spectra. A bright homogeneous walkway was used as the reference area. (iv) The estimation of relative spectral response functions (SRFs) can be formulated as a constrained least-squares problem [?]. Reflectance conversion coefficients of the RGB image are simultaneously obtained. (v) The RGB image is converted to reflectance using the co-efficients.

2.2. Extended CNMF

After the preprocessing, the high-spatial-resolution HS data is obtained by extended CNMF. Since the difference in GSDs is 10-fold and only three spectral channels are available for higher-spatial-resolution information, the unmixing of the RGB image is a severely ill-posed problem. To tackle this challenging problem, we improve the initialization of the abundance matrix ($\mathbf{A}$) in the unmixing of the RGB image.

CNMF starts with NMF-based unmixing of the HS data to estimate the endmember ($\mathbf{E}$) and abundance ($\mathbf{A}_h$) matrices using its spectral advantage. NMF converges to local minima; therefore, the initialization is important. The vertex component analysis (VCA) [8] and fully constrained least-squares (FCLS) [9] methods are used for the initialization of $\mathbf{E}$ and $\mathbf{A}_h$, respectively.

Next, the RGB image is unmixed by NMF after initializing the endmember ($\mathbf{E}_m$) and abundance ($\mathbf{A}$) matrices using $\mathbf{E}$ and $\mathbf{A}_h$. The relative SRFs ($\mathbf{R}$) are used for initializing $\mathbf{E}_m$. In the ordinary CNMF, $\mathbf{A}$ is initialized as interpolated abundance maps calculated from $\mathbf{A}_h$, which is not suitable for the 10-fold GSD difference. In this work, we introduce segmentation for better initialization of $\mathbf{A}$, as shown in Fig. 2. The interpolated abundance maps are converted to segmented abundance maps by integrating region-unifying segmentation of the RGB image with the interpolated abundance maps. The

Fig. 3. 719 nm band images of (left) HS and (right) fused data. Subimages A and C show tree crowns and B shows the plastic sheet.

average abundance value of a segment is assigned to all pixels in the segment. Finally, a blurred version of segmented abundances is used for initializing $\mathbf{A}$. In addition, we update only $\mathbf{A}$ in RGB unmixing to avoid the incorrect convergence of $\mathbf{E}_m$ owing to the small number of spectral bands.

The sequential unmixing for HS data is processed after initializing the abundance by $\mathbf{A}_h = \mathbf{AS}$. After that, two datasets are alternately unmixed until convergence and the fused data is obtained by multiplying the endmember matrix by the high-spatial-resolution abundance matrix.

2.3. Target Detection

To examine the effectiveness of unmixing-based HS super-resolution for practical applications, we use the fused data for target detection. Our target is the green plastic sheet and its spectrum is obtained by ground measurements using an USB2000+VIS-NIR (Ocean Optics Inc.). We adopt a sub-pixel target detection method based on linear spectral unmixing named *nonnegatively constrained least squares* (NCLS) [10]: 1) The target spectrum is set as the first endmember $\mathbf{E} = [\mathbf{e}_0]$. Let $k = 0$ and select ϵ to be a prescribed error threshold. 2) Let $k \leftarrow k + 1$ and the abundance fractions are estimated with the endmember matrix $\mathbf{E} = [\mathbf{e}_0...\mathbf{e}_{k-1}]$ by solving the NCLS problem:

$$\min_{\mathbf{a}} \frac{1}{2}\|\mathbf{z} - \mathbf{Ea}\|_2^2 \text{ subject to } \mathbf{a} \succeq 0, \quad (4)$$

3) Check the least squares error if $\|\mathbf{z} - \mathbf{Ea}\|_2^2 < \epsilon$ for all $\mathbf{z}$. If it is, the algorithm stops, otherwise continue. 4) Find a new endmember as
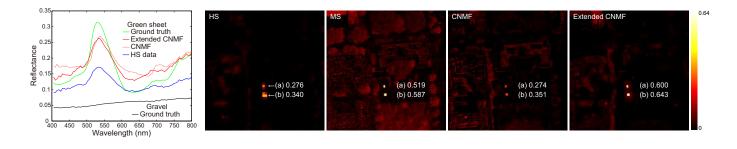
$$\mathbf{e}_k = \operatorname*{argmax}_{\mathbf{z}} \|\mathbf{z} - \mathbf{Ea}\|_2^2 \quad (5)$$

3. EXPERIMENTAL RESULTS

We produced the 0.25-m-GSD HS data with 97 bands over the 400–800 nm spectral region by applying the extended CNMF to the HS and RGB images. Fig. 3 shows 719-nm-band images of low-spatial-resolution HS and fused data. As shown in the enlarged images in Fig. 3, tree crowns and the green plastic sheet spread on the roof are identifiable with the fused data owing to the 10-fold improvement of GSD.

To evaluate the spectral reconstruction of the fused data, we examine the spectral profile of the green plastic sheet shown in Fig. 3. The left graph in Fig. 4 shows the spectra of the green plastic sheet for low-spatial-resolution HS and for CNMF and extended-CNMF data as well as the ground-measured spectra of the green plastic sheet and the surrounding gravel. The spectrum of the low-spatial-resolution HS data appears to be a mixture of the two ground-measured spectra because of mixed pixels. In contrast, the peak around the green region is restored for the extended-CNMF data, whereas the CNMF spectrum contains artificial errors. This result indicates that the segmentation-integrated initialization of higher-spatial-resolution abundance maps contributes to a better convergence of the RGB-image unmixing, which enables the restoration of pure spectra. The difference between the extended-CNMF and ground-measured spectra may be caused by errors in the preprocessing or in the ground measurements.

Next, we applied the NCLS subpixel target detection to HS, MS, CNMF, and extended-CNMF datasets and the target abundances are shown at the right images of Fig. 4. The abundances at the green plastic sheets obtained by the extended-CNMF data show higher values compared to those of the other data. The clearer abundance contrast between the target objects and backgrounds is expected to contribute to better target detection. Surprisingly, the abundances of the target objects obtained by the CNMF data show lower values com-

Fig. 4. (Left) Spectral validation of fused data using ground-measured spectra. Right images show abundance maps of green plastic sheet for HS, MS, CNMF, and extended CNMF data with two peak values.

pared to the HS and MS data because of spectral errors. It suggests that the careful preprocessing and the extended-CNMF are effective in practical use with challenging optimization conditions.

4. CONCLUSION

In this work, we presented an airborne experiment of unmixing-based HS super-resolution using an RGB image to examine the restoration of pure spectra and its effect on target detection. We introduced segmentation to the initialization of higher-spatial-resolution abundance maps in CNMF to deal with a severe ill-posed problem due to the 10-fold GSD difference and lack of higher-spatial-resolution near-infrared image in the MS data. The extended CNMF method not only improved the spatial resolution but also restored pure spectra, which contributes to accurate target detection.

5. REFERENCES

[1] R. C. Hardie, M. T. Eismann, and G. L. Wilson, "Map estimation for hyperspectral image resolution enhancement using an auxiliary sensor," *IEEE Trans. Image Processing*, vol. 13, no. 9, pp. 1174–1184, 2004.

[2] M. T. Eismann and R. C. Hardie, "Application of the stochastic mixing model to hyperspectral resolution enhancement," *IEEE Trans. Geosci. Remote Sens.*, vol. 42, no. 9, pp. 1924–1933, 2004.

[3] N. Yokoya, T. Yairi, and A. Iwasaki, "Coupled nonnegative matrix factorization unmixing for hyperspectral and multispectral data fusion," *IEEE Trans. Geosci. Remote Sens.*, vol. 50, no. 2, pp. 528–537, 2012.

[4] D. D. Lee and H. S. Seung, "Learning the parts of objects by nonnegative matrix factorization," *Nature*, vol. 401, pp. 788–791, 1999.

[5] N. Yokoya, N. Mayumi, and A. Iwasaki, "Cross-calibration for data fusion of EO-1/Hyperion and Terra/ASTER," *IEEE J. Sel. Topics Appl. Earth Observ. Remote Sens.*, vol. 6, no. 2, pp. 419–426, 2013.

[6] N. Yokoya, N. Miyamura, and A. Iwasaki, "Detection and correction of spectral and spatial misregistrations for hyperspectral data using phase correlation method," *Applied Optics*, vol. 49, no. 24, pp. 4568–4575, 2010.

[7] G. D. Finlayson, S. Hordley, and P. M. Hubel. "Recovering device sensitivities with quadratic programming," in *Proc. the IS and T/SID Sixth Color Imaging Conference: Color Science, Systems, and Applications*, pp. 90–95, 1998.

[8] J. M. P. Nascimento and J. M. B. Dias, "Vertex component analysis: A fast algorithm to unmix hyperspectral data," *IEEE Trans. Geosci. Remote Sens.*, vol. 43, no. 4, pp. 898–910, 2005.

[9] D. C. Heinz and C.-I. Chang, "Fully constrained least squares linear spectral mixture analysis method for material quantification in hyperspectral imagery," *IEEE Trans. Geosci. Remote Sens.*, vol. 39, no. 3, pp. 529–545, 2001.

[10] C.-I. Chang and D. C. Heinz, "Constrained sub pixel target detection for remotely sensed imagery," vol. 38, no. 3, pp. 1144–1159, 2000.